

C-loss based Higher-order Fuzzy Inference Systems for Identifying DNA N4-methylcytosine Sites

Yijie Ding, Prayag Tiwari^b, Quan Zou, Fei Guo, and Hari Mohan Pandey^b

Abstract—DNA methylation is an epigenetic marker, that plays an important role in the biological processes of regulating gene expression, maintaining chromatin structure, imprinting genes, inactivating X chromosomes, and developing embryos. The traditional detection method is time-consuming. Currently, researchers have used effective computational methods to improve the efficiency of methylation detection. This study proposes a fuzzy model with correntropy induced loss (C-loss) function to identify DNA N4-methylcytosine (4mC) sites. To improve the robustness and performance of the model, we use kernel method and the C-loss function to build a higher-order fuzzy inference systems (HFIS). To test performance, our model is implemented on six 4mC and eight UCI data sets. The experimental results show that our model achieves better prediction performance.

Index Terms—DNA N4-methylcytosine, 4mC, Fuzzy model, Kernel method, Sequence classification.

I. INTRODUCTION

DNA N4-methylcytosine (4mC) is a form of DNA chemical modification that can change genetic performance without changing the DNA sequence. A large number of studies have shown that DNA methylation can control gene expression by changing the chromatin structure, DNA conformation, DNA stability, and DNA interactions with proteins. In the development of malignant tumors, the state of methylation is not static. The degree of hypomethylation of the whole genome in tumor cells is closely related to disease progression, tumor size, and malignancy. DNA methylation detection is effective for assessing tumor malignancy. The degree of judgment is of great significance. However, the traditional detection method is a wet experiment, which is time-consuming and labor-intensive. Therefore, it is necessary to propose an effective computational method for 4mC site identification.

This work is supported in part by the National Natural Science Foundation of China (NSFC 62172076, 62172296 and 61902271), the Natural Science Research of Jiangsu Higher Education Institutions of China (19KJB520014) and the Special Science Foundation of Quzhou (2021D004). (Corresponding Author: Quan Zou, Fei Guo, Hari Mohan Pandey, and Prayag Tiwari)

Y. Ding is with Yangtze Delta Region Institute (Quzhou), University of Electronic Science and Technology of China, Quzhou, 324000, P.R.China; E-mail: wuxi_dyj@163.com

P. Tiwari is with the Department of Computer Science, Aalto University, Espoo, Finland; Email: prayag.tiwari@aalto.fi

Q. Zou is with the Institute of Fundamental and Frontier Sciences, University of Electronic Science and Technology of China, Chengdu, 610054, P.R.China; E-mail: zouquan@nclab.net

F. Guo is with the School of Computer Science and Engineering, Central South University, Changsha, 410083, P.R.China; E-mail: guofeieileen@163.com

H.M. Pandey is with Data Science and Artificial Intelligence, Department of Information and Computing, Bournemouth University, UK; Email: profhari-mohanpandey@gmail.com

Manuscript received Nov 28, 2021; revised , .

In recent years, computational methods based on machine learning (ML) have been proposed to solve 4mC recognition [1], [2], [3]. Conventional statistical learning and deep learning are the two main methods used to solve the 4mC identification problem. For statistical learning methods, manual feature extraction was used to represent DNA sequences. The support vector machine (SVM) [4], random forest (RF), naive Bayes, extremely randomized tree, AdaBoost and logistic regression were utilized to build a predictive model. The iDNA4mC model was first proposed to identify 4mC sites by Chen et al. [5]. The iDNA4mC used nucleotide chemical properties and frequency to represent features of DNA and fed them into SVM for prediction. He et al. [6] developed 4mCPred via SVM and position-specific trinucleotide sequence propensity (PSTNP), which can extract key information of DNA sequences. Wei et al. [7] proposed a two-step feature optimization strategy to construct a predictive model. This method was called 4mCPred-SVM. Based on multiple features of DNA sequences, Hasan et al. developed two types of predictors, i4mC-ROSE[8] and i4mC-Mouse [9], to identify 4mC sites in Rosaceae and mouse genomes. To further improve the predictive performance of the model, iDNA-MS[10], Meta-4mCpred [11] and DNA4mC-LIP [12] integrated existing predictors to identify 4mC sites.

Deep learning can represent the features of DNA sequences through multilayer networks. The 4mCCNN model, which was based on one-dimensional convolutional neural network (CNN), was proposed by Khanal et al. [13]. The DNC4mC-Deep model [14] employed nucleotide frequency (NCPNF), nucleotide chemical property, binary encoding (BE), nucleotide chemical property (NCP) and Kmer as input features for CNN. The long short-term memory (LSTM) was also used to develop an effective deep model, called DeepTorrent [15].

Fuzzy inference system (FIS) is an effective calculation model to solve uncertain and vague problems. Zero-order and first-order FIS (1-FIS), which are two of the more popular FIS models, had been employed in data mining, pattern recognition and automatic control. Classical fuzzy inference systems have three types of models: Mamdani-Larsen [16], Takagi-Sugeno-Kang (TSK) [17], [18] and generalized fuzzy systems [19]. Among them, the TSK model is a popular fuzzy system. Chen [20] and Chiang [21] proposed the zero-order TS fuzzy systems based on SVM. Support vectors were used to construct the antecedent and subsequent parts of fuzzy rules; the kernel function of SVM was composed of fuzzy basis functions, and the number of fuzzy rules was determined by the number of support vectors (consistent). This method can improve generalization ability, but with an increase in the support vector, the fuzzy rules will also increase. Therefore,

this strategy increased the complexity of the systems. Xu et al. [22] also developed a zero-order TS fuzzy systems, called enhanced soft subspace clustering and sparse learning-based concise TSK fuzzy systems (ESSC-SL-CTSK-FS), could generate the sparse subspace and antecedent in each fuzzy rule. Kerk et al. [23] developed a monotone zero-order TSK-based FIS via monotone fuzzy rule interpolation. The first-order TSK fuzzy systems used fuzzy clustering algorithm to construct the rule antecedent, and the latter was a linear function. When the data is insufficient, or a fuzzy system trained with an incomplete data set, the generalization ability of the model will be affected. To overcome this problem, Deng et al. [24] studied a fuzzy system based on knowledge-levers (KL-FS) from the perspective of transfer learning. Gu et al. [25] proposed Bayesian TSK fuzzy classifier (B-TSK-FC), which estimated the parameters by Markov-Chain Monte-Carlo technique. Rezaee [26] developed a data-driven TSK systems that automatically obtained the fuzzy rules and optimized parameters. To address the problem of regression, Zuo et al. [27] proposed a TS fuzzy regression transfer learning model. For the constrained monotonic scenarios, a monotonic relation-constrained TSK systems were proposed by Deng [28]. For the data sequence, it is more difficult to determine the fuzzy set and adapt changes in the data distribution. Yu et al. [29] designed a topology learning-based fuzzy random neural network (TLFRNN) to solve this problem. To improve the performance of predictive model, a patch learning (PL) algorithm was proposed to build fuzzy systems by Wu et al. [30]. For TSK systems, Wu et al. [31] also proposed an efficient and effective training algorithm with minibatch gradient descent (MBGD), AdaBound and regularization. For identification of epileptic EEG signals, Jiang et al. designed a multiview TSK fuzzy systems (MV-TSK-FS) [32], which weighted outputs of different views. Jiang also employed TSK fuzzy systems, semisupervised learning and transductive transfer learning models to detect epileptic seizures via EEG signals [33]. Wiktorowicz [34] constructed a high-order TSK fuzzy systems by the particle swarm optimization (PSO) and batch least squares (BLS).

Although, FIS (based on TSK fuzzy systems) has been significantly developed, the above works lack consideration for the processing of high-dimensional feature spaces and noise samples. As the dimension of the feature space increases, the complexity of FIS will also increase. Noise samples will also affect the decision hyperplane of the model. Inspired by Chen [20], Chiang [21] and Wiktorowicz's [34] works, we propose a correntropy induced loss-based kernelized higher-order FIS (C-KHFIS), which is an extension of TSK fuzzy systems [17], [18]. The correntropy induced loss (C-loss) function [35] was a loss function that could improve robustness against noise for classifier.

The contributions of this work are as follows:

- (1) We use the fuzzy rule-based kernel to build a higher-order fuzzy inference systems, which is a kernelized model.
- (2) C-loss function is employed to improve the generalization ability of fuzzy systems.

- (3) An effective iterative algorithm is proposed to optimize our fuzzy systems.

This work is organized as follows: In section II, we introduce first-order and high-order FIS models. In section III, we propose a C-loss based higher-order fuzzy inference systems. In section IV, we introduce the feature extraction of DNA sequences. In section V, we test our method on several benchmark data sets. Finally, the conclusion and future work are given in section VI.

II. RELATED WORK

FIS is a nonlinear system, which is described by multiple sets of if-then fuzzy rules. Each subsystem (corresponding to each rule) is a local approximation to the target problem. Finally, multiple subsystems are combined to jointly approximate the objective function. By the fuzzy C-means (FCM) algorithm, the subsystems of each fuzzy set obtain the distribution of local samples. Compared with the traditional neural network based on the backpropagation algorithm, FIS can reduce the computational complexity of the model via local approximation.

A. First-order fuzzy inference systems

Suppose there is a training set $\mathbf{X} = [\mathbf{x}_1, \dots, \mathbf{x}_i, \dots, \mathbf{x}_N] \in \mathbf{R}^{d \times N}$ with N samples and d dimensions, where $\mathbf{x}_i = (x_{i1}, x_{i2}, \dots, x_{id})^T \in \mathbf{R}^{d \times 1}$. In first-order fuzzy systems, the k -th fuzzy rule R_k can be represented as:

$$\begin{aligned} & \text{If } x_{i1} \text{ is } A_1^k \wedge x_{i2} \text{ is } A_2^k \wedge \dots \wedge x_{id} \text{ is } A_d^k, \\ & \text{Then } f^k(\mathbf{x}_i) = p_0^k + p_1^k x_{i1} + p_2^k x_{i2} + \dots + p_d^k x_{id}, \quad (1) \\ & k = 1, 2, \dots, M, \end{aligned}$$

where M denotes the number of fuzzy rules. A_j^k is the k -th fuzzy set for the j -th input feature x_{ij} , \wedge represents a fuzzy conjunction, and $f^k(\mathbf{x}_i)$ denotes the defuzzification function for local output under k -th fuzzy set. In fact, $f^k(\mathbf{x}_i)$ is a first-order polynomial. When $f^k(\mathbf{x}_i)$ is nonlinear function, the above fuzzy systems belong to higher order fuzzy inference systems. The decision formula of first-order FIS (1-FIS) can be represented as:

$$\begin{aligned} y(\mathbf{x}_i) &= \sum_{k=1}^M \frac{\mu^k(\mathbf{x}_i)}{\sum_{k'=1}^M \mu^{k'}(\mathbf{x}_i)} f^k(\mathbf{x}_i) \\ &= \sum_{k=1}^M \tilde{\mu}^k(\mathbf{x}_i) f^k(\mathbf{x}_i), \quad (2) \end{aligned}$$

where

$$\mu^k(\mathbf{x}_i) = \prod_{j=1}^d \mu_{A_j^k}(x_{ij}), \quad (3a)$$

$$\tilde{\mu}^k(\mathbf{x}_i) = \frac{\mu^k(\mathbf{x}_i)}{\sum_{k'=1}^M \mu^{k'}(\mathbf{x}_i)}, \quad (3b)$$

where $\mu_{A_j^k}(x_{ij})$ denotes the fuzzy membership function, which can be calculated by Gaussian function:

$$\mu_{A_j^k}(x_{ij}) = \exp\left(-\frac{(x_{ij} - c_j^k)^2}{2\sigma_j^k}\right), \quad (4)$$

172 where σ_j^k and c_j^k are the center and variance of k -th fuzzy
 173 set in j -th dimension and $\sum_{k=1}^M \tilde{\mu}^k(\mathbf{x}_i) \neq 0$. The models con-
 174 structed from Gaussian membership function can approximate
 175 nonlinear continuous systems with arbitrary precision, and this
 176 type of membership function has been widely used in the field
 177 of fuzzy control.

178 For 1-FIS, the parameters of σ_j^k and c_j^k are in the if-parts.
 179 $\mathbf{p}^k = [p_0^k, p_1^k, \dots, p_d^k]^T \in \mathbf{R}^{(1+d) \times 1}$ are the parameters of then-
 180 parts. The learning of the above two kinds of parameters is
 181 implemented independently. For if-parts, FCM algorithm [36]
 182 is utilized to estimate σ_j^k and c_j^k :

$$c_j^k = \frac{\sum_{i=1}^N \mu_{ik} x_{ij} \sum_{i=1}^N \mu_{ik}}{\sum_{i=1}^N \mu_{ik}}, \quad (5a)$$

$$\sigma_j^k = \frac{1}{2} \sum_{i=1}^N \mu_{ik} (x_{ij} - c_j^k)^2 \sum_{i=1}^N \mu_{ik}, \quad (5b)$$

183 where μ_{ik} is the membership value of sample \mathbf{x}_i belonging
 184 to cluster k . After if-parts learning, the parameters of of σ_j^k
 185 and c_j^k are determined. Next, the parameters of then-parts can
 186 be obtained by least squares method. Let the output of k -th
 187 fuzzy rule be:

$$\tilde{\mathbf{x}}_i^k = \tilde{\mu}^k(\mathbf{x}_i) \mathbf{x}_e \in \mathbf{R}^{(1+d) \times 1}, \quad (6a)$$

$$\mathbf{x}_e = (1, (\mathbf{x}_i^T)^T) \in \mathbf{R}^{(1+d) \times 1}. \quad (6b)$$

188 Therefore, the output of M fuzzy rules can be represented
 189 as follows:

$$\mathbf{x}_{gi} = \left((\tilde{\mathbf{x}}_i^1)^T, (\tilde{\mathbf{x}}_i^2)^T, \dots, (\tilde{\mathbf{x}}_i^M)^T \right)^T \in \mathbf{R}^{[(1+d)*M] \times 1}. \quad (7)$$

190 For the k -th fuzzy rule, the the parameters of then-parts
 191 are defined as:

$$\mathbf{p}^k = (p_0^k, p_1^k, \dots, p_d^k)^T \in \mathbf{R}^{(1+d) \times 1}. \quad (8)$$

192 The parameters of M then-parts are defined as:

$$\mathbf{p}_g = ((\mathbf{p}^1)^T, (\mathbf{p}^2)^T, \dots, (\mathbf{p}^M)^T)^T \in \mathbf{R}^{[(1+d)*M] \times 1}. \quad (9)$$

193 The output of the first-order fuzzy systems can be rewritten
 194 as:

$$y(\mathbf{x}_i) = \mathbf{p}_g^T \mathbf{x}_{gi}. \quad (10)$$

195 Then-parts learning can be regarded as a linear regression
 196 problem:

$$J_{1-FIS}(\mathbf{p}_g) = \frac{\lambda}{2} \|\mathbf{p}_g\|_2^2 + \frac{1}{2} \sum_{i=1}^N \|\mathbf{p}_g^T \mathbf{x}_{gi} - y_i\|_2^2. \quad (11)$$

B. Higher-order FIS

197 For the higher-order FIS, the k -th fuzzy rule R_k can be
 198 represented as: 199

If x_{i1} is $A_1^k \wedge x_{i2}$ is $A_2^k \wedge \dots \wedge x_{id}$ is A_d^k ,

Then $f^k(\mathbf{x}_i) = p_0^k + \sum_{j=1}^d p_j^k x_{ij} + \sum_{j,h}^d p_{jh}^k x_{ij} x_{ih} + \dots$ (12)

$$+ \sum_{j_1, j_2, \dots, j_m=1}^d p_{j_1, \dots, j_m}^k x_{ij_1} x_{ij_2} \dots x_{ij_m},$$

$k = 1, 2, \dots, M$,

200 where $m \geq 2$ is the degree of a higher-order polynomial, which
 201 means that the functions are nonlinear. 202

203 1-FIS, which is based on TSK fuzzy systems, uses multiple
 204 linear systems to fit a nonlinear system and a fuzzy algorithm
 205 to deconstruct the input variables. Then, the variables are
 206 defuzzified through fuzzy calculus inference to generate the
 207 equation of the relationship between inputs and outputs. The
 208 identification of 4mC site is a complex classification problem.
 209 We conduct research on the basis of 1-FIS and propose a C-loss
 based higher-order fuzzy inference system.

III. C-LOSS BASED HIGHER-ORDER FUZZY INFERENCE SYSTEMS

A. Kernelized higher-order fuzzy inference systems

210 The kernelized higher-order fuzzy inference systems (KHFIS)
 211 can actually be regarded as a nonlinear problem, which
 212 can be decomposed into M local nonlinear submodels. To
 213 obtain the form of the then-part function $f^k(\mathbf{x}_i)$ for the
 214 nonlinear submodel, we introduce the mapping function $\phi(\cdot)$ for
 215 $\phi(\mathbf{x}_i)^T \phi(\mathbf{x}_j) = K(\mathbf{x}_i, \mathbf{x}_j)$ (kernel), where $K(\mathbf{x}_i, \mathbf{x}_j)$ can be
 216 constructed by a linear, radial basis function (RBF), polynomial.
 217 The k -th fuzzy rule of the KHFIS can be represented as: 218

If $\mathbf{x}_i \in A_1^k \wedge x_{i2}$ is $A_2^k \wedge \dots \wedge x_{id}$ is A_d^k ,

Then $f^k(\mathbf{x}_i) = \tilde{\mu}^k(\mathbf{x}_i) (\mathbf{p}^k)^T (1, \phi(\mathbf{x}_i)^T)^T$, (13)

$k = 1, 2, \dots, M$.

219 Thus, the output of the higher-order FIS is: 220

$$f(\mathbf{x}_i) = \sum_{k=1}^M \tilde{\mu}^k(\mathbf{x}_i) (\mathbf{p}^k)^T (1, \phi(\mathbf{x}_i)^T)^T. \quad (14)$$

221 The nonlinear problem of higher-order FIS is decomposed
 222 into a linear combination of M local submodels in a high-
 223 dimensional space. Suppose the output of the M if-parts is
 224 Φ_{gi} : 225

$$\Phi_{gi} = \{ (\psi(\mathbf{x}_i)^1)^T, \dots, (\psi(\mathbf{x}_i)^k)^T, \dots, (\psi(\mathbf{x}_i)^M)^T \}^T \in \mathbf{R}^{[(1+d')*M] \times 1}, \quad (15)$$

$$\psi(\mathbf{x}_i)^k = \tilde{\mu}^k(\mathbf{x}_i) ((1, \phi(\mathbf{x}_i)^T)^T) \in \mathbf{R}^{(1+d') \times 1},$$

$$k = 1, 2, \dots, M,$$

226 where $\psi(\mathbf{x}_i)^k$ is the output of the k -th if-parts and d' is the
 227 dimension of nonlinear projection. The objective function of
 228 KHFIS is:

$$\begin{aligned}
 J_{KHFIS}(\mathbf{p}_g) &= \frac{\lambda}{2} \|\mathbf{p}_g\|_2^2 \\
 &+ \frac{1}{2} \sum_{i=1}^N \|\mathbf{p}_g^T \Phi_{gi} - y_i\|_2^2,
 \end{aligned} \tag{16}$$

where $\mathbf{p}_g \in \mathbf{R}^{[(1+d')*M] \times 1}$.

We set $y_i - \mathbf{p}_g^T \Phi_{gi} = \xi_i$ and Eq. (16) can be rewritten as:

$$\begin{aligned}
 \min J(\mathbf{p}_g, \xi_i) &= \frac{1}{2} \mathbf{p}_g^T \mathbf{p}_g + \frac{1}{2\lambda} \sum_{i=1}^N \xi_i^2, \\
 \text{s.t. } y_i - \mathbf{p}_g^T \Phi_{gi} &= \xi_i, \quad i = 1, 2, \dots, N.
 \end{aligned} \tag{17}$$

The Lagrangian function of the optimization problem (17) is:

$$\begin{aligned}
 L(\mathbf{p}_g, \xi_i, \alpha_i) &= \frac{1}{2} \mathbf{p}_g^T \mathbf{p}_g + \frac{1}{2\lambda} \sum_{i=1}^N \xi_i^2 \\
 &- \sum_{i=1}^N \alpha_i (\xi_i - y_i + \mathbf{p}_g^T \Phi_{gi}),
 \end{aligned} \tag{18}$$

where $\alpha_i, i = 1, 2, \dots, N$ is the Lagrange multiplier. The partial derivatives of L is found by:

$$\begin{cases}
 \partial L / \partial \mathbf{p}_g = 0 & \Rightarrow \mathbf{p}_g = \sum_{i=1}^N \alpha_i \Phi_{gi}, \\
 \partial L / \partial \xi_i = 0 & \Rightarrow \xi_i = \lambda \alpha_i, \\
 \partial L / \partial \alpha_i = 0 & \Rightarrow \mathbf{p}_g^T \Phi_{gi} + \xi_i - y_i = 0.
 \end{cases} \tag{19}$$

Similar to TSK fuzzy systems, KHFIS uses a two-step learning strategy. First, the FCM algorithm (unsupervised learning stage) is used to initialize the fuzzy subset; then the supervised learning method is employed to train the parameters of the model according to the error. In Eq. (19), the solution process is the supervised learning stage of our algorithm. We can obtain the following linear equation:

$$(\Omega + \lambda \mathbf{I}) \alpha = \mathbf{y}, \tag{20}$$

where $\alpha = (\alpha_1, \alpha_2, \dots, \alpha_N)^T$ and $\mathbf{y} = (y_1, y_2, \dots, y_N)^T$. $\Omega = \Phi_g^T \Phi_g \in \mathbf{R}^{N \times N}$ is a symmetric matrix, which can be called the fuzzy kernel. $\Phi_g = \{\Phi_{g1}, \dots, \Phi_{gi}, \dots, \Phi_{gN}\} \in \mathbf{R}^{[(1+d')*M] \times N}$. Ω_{ij} can be calculated by:

$$\begin{aligned}
 \Omega_{ij} &= \Phi_{gi}^T \Phi_{gj} \\
 &= \left[(\psi(\mathbf{x}_i)^1)^T, \dots, (\psi(\mathbf{x}_i)^M)^T \right]_{1 \times [(1+d')*M]} \\
 &\quad \begin{bmatrix} \psi(\mathbf{x}_j)^1 \\ \vdots \\ \psi(\mathbf{x}_j)^M \end{bmatrix}_{[(1+d')*M] \times 1} \\
 &= \sum_{k=1}^M (\psi(\mathbf{x}_i)^k)^T \psi(\mathbf{x}_j)^k \\
 &= \sum_{k=1}^M \tilde{\mu}^k(\mathbf{x}_i) \tilde{\mu}^k(\mathbf{x}_j) \left[1, \phi(\mathbf{x}_i)^T \right]_{1 \times (1+d')} \begin{bmatrix} 1 \\ \phi(\mathbf{x}_j) \end{bmatrix}_{(1+d') \times 1} \\
 &= \sum_{k=1}^M \tilde{\mu}^k(\mathbf{x}_i) \tilde{\mu}^k(\mathbf{x}_j) (\phi(\mathbf{x}_i)^T \phi(\mathbf{x}_j) + 1) \\
 &= \sum_{k=1}^M \tilde{\mu}^k(\mathbf{x}_i) \tilde{\mu}^k(\mathbf{x}_j) (K(\mathbf{x}_i, \mathbf{x}_j) + 1),
 \end{aligned} \tag{21}$$

where $\tilde{\mu}^k(\mathbf{x}_i) \tilde{\mu}^k(\mathbf{x}_j) (K(\mathbf{x}_i, \mathbf{x}_j) + 1)$ can be considered as the element of the fuzzy kernel in the k -th fuzzy rule.

The kernel can be constructed by the radial basis function (RBF):

$$K_{RBF}(\mathbf{x}_i, \mathbf{x}_j) = \exp(-\gamma \|\mathbf{x}_i - \mathbf{x}_j\|^2), \tag{22}$$

where γ denotes the kernel parameters. By a high-dimensional dot product calculation, the RBF kernel function can project samples from a low-dimensional space to a high-dimensional space. The value of the RBF function is a good similarity measure representation, and the range is between 0 and 1. The value increases with decreasing Euclidean distance.

For a test sample $\mathbf{x}_t \in \mathbf{R}^{d \times 1}$, the final output of KHFIS is:

$$\begin{aligned}
 y(\mathbf{x}_t) &= \mathbf{p}_g^T \Phi_{gt} \\
 &= \sum_{i=1}^N \alpha_i \left[(\psi(\mathbf{x}_i)^1)^T, \dots, (\psi(\mathbf{x}_i)^M)^T \right]_{1 \times [(1+d')*M]} \\
 &\quad \begin{bmatrix} \psi(\mathbf{x}_t)^1 \\ \vdots \\ \psi(\mathbf{x}_t)^M \end{bmatrix}_{[(1+d')*M] \times 1} \\
 &= \sum_{i=1}^N \alpha_i \sum_{k=1}^M \tilde{\mu}^k(\mathbf{x}_i) \tilde{\mu}^k(\mathbf{x}_t) (K(\mathbf{x}_i, \mathbf{x}_t) + 1).
 \end{aligned} \tag{23}$$

For binary classification ($y \in \{+1, -1\}$), Eq. (23) can also be represented as:

$$y(\mathbf{x}_t) = \text{sign} \left[\sum_{i=1}^N \alpha_i \sum_{k=1}^M \tilde{\mu}^k(\mathbf{x}_i) \tilde{\mu}^k(\mathbf{x}_t) (K(\mathbf{x}_i, \mathbf{x}_t) + 1) \right]. \tag{24}$$

The process of KHFIS is shown in Algorithm 1 and Fig. 1.

Algorithm 1 Algorithm of KHFIS

Require: The training labels $\mathbf{y} \in \mathbf{R}^{N \times 1}$, features $\mathbf{X} = [\mathbf{x}_1, \dots, \mathbf{x}_i, \dots, \mathbf{x}_N] \in \mathbf{R}^{d \times N}$ and testing sample $\mathbf{x}_t \in \mathbf{R}^{d \times 1}$; The parameters of regularization coefficient λ , number of fuzzy rules M ;

Ensure: The prediction of $y(\mathbf{x}_t)$;

- 1: Using FCM to calculate the parameters of if-parts;
 - 2: Estimating $\tilde{\mu}^k(\mathbf{x}_i), i = 1, 2, \dots, N, k = 1, 2, \dots, M$ by Eq. (3a) and (3b);
 - 3: Computing Ω by Eq. (22) and (21);
 - 4: Estimating α via Eq. (20).
 - 5: Predicting $y(\mathbf{x}_t)$ by Eq. (23);
-

B. Correntropy induced loss based KHFIS

The C-loss function [35] can be expressed as:

$$l_C(y_i, f(\mathbf{x}_i)) = 1 - \exp\left(-\frac{(y_i - f(\mathbf{x}_i))^2}{2\rho^2}\right), \tag{25}$$

where ρ denotes the bandwidth. The C-loss is differentiable and smooth. Fig. 2 shows the square loss and C-loss function under different widths ρ . Obviously, the C-loss function can effectively reduce the influence of large errors on the model. The square loss increases as the error increases (the negative error decreases), and the value of the loss function increases

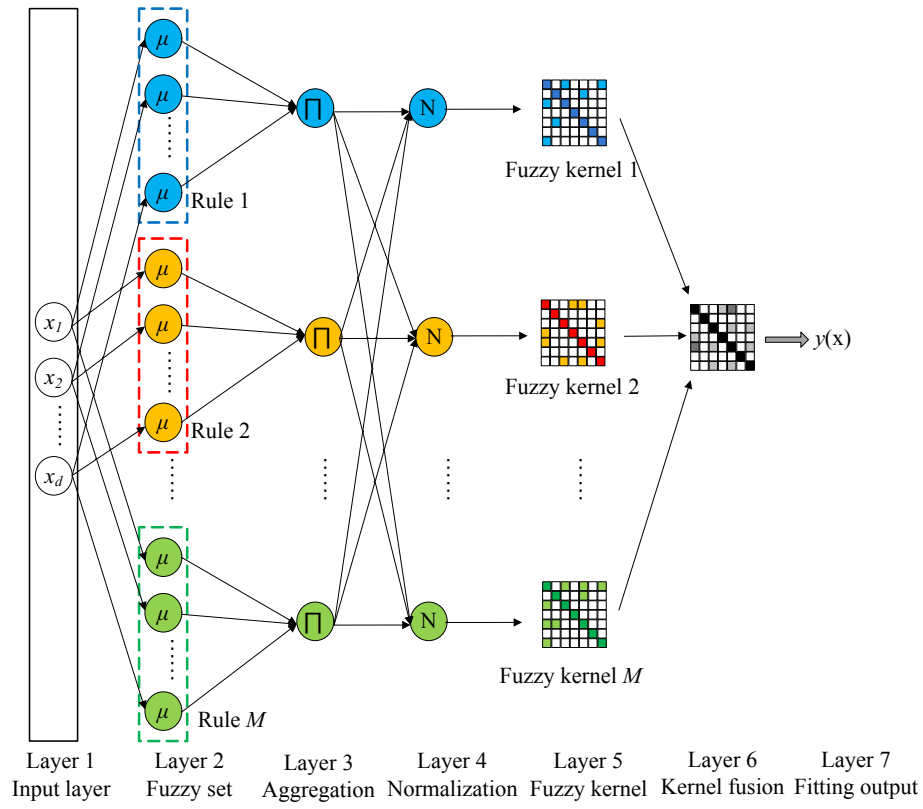


Fig. 1: Schematic of kernelized higher-order fuzzy inference systems.

268 quickly. In contrast, the incremental slope of the C-loss function
 269 is not as steep. We can adjust the width ρ to adapt the sensitivity
 270 to outliers.

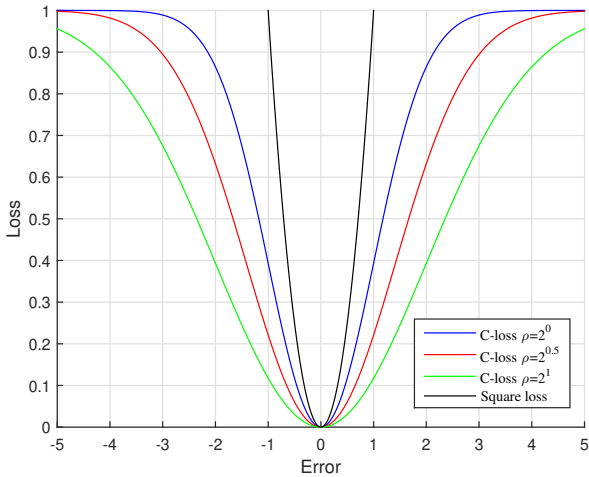


Fig. 2: C-loss with different widths.

271 We replace the square loss function with the C-loss function,
 272 and the mathematical model of the C-loss based KHFIIS (C-
 273 KHFIIS) is defined as:

$$\begin{aligned} \min J(\mathbf{p}_g, \xi_i) &= \frac{1}{2} \mathbf{p}_g^T \mathbf{p}_g \\ &+ \frac{1}{2\lambda} \sum_{i=1}^N \left(1 - \exp\left(-\frac{\xi_i^2}{2\rho^2}\right) \right), \quad (26) \\ \text{s.t. } y_i - \mathbf{p}_g^T \Phi_{gi} &= \xi_i, \quad i = 1, 2, \dots, N. \end{aligned}$$

274 However, Eq. (26) is nonconvex and cannot be solved directly.
 275 The half-quadratic (HQ) optimization algorithm [37] can be
 276 used to solve the above problem. By introducing an auxiliary
 277 variable, we first define a convex function:

$$g(\nu) = -\nu \log(-\nu) + \nu, \quad (27)$$

278 where $\nu < 0$. The conjugate function of $g(\nu)$ is:

$$g^*(\tau) = \sup_{\nu} g'(\nu), \quad (28)$$

279 where

$$g'(\nu) = \tau\nu - g(\nu) = \tau\nu + \nu \log(-\nu) - \nu, \quad (29)$$

280 When $g'(\nu)$ is a nonconvex function, let $\frac{dg'(\nu)}{d\nu} = 0$:

$$\tau + \log(-\nu) = 0 \Rightarrow \nu = -\exp(-\tau) < 0. \quad (30)$$

281 When formula (30) is combined into formula (28):

$$g^*(\tau) = \exp(-\tau). \quad (31)$$

282 Letting $\tau = \frac{\xi_i^2}{2\rho^2}$, we can obtain:

$$g^* \left(\frac{\xi_i^2}{2\rho^2} \right) = \sup_{\nu} \left\{ \frac{\xi_i^2}{2\rho^2} \nu + \nu \log(-\nu) - \nu \right\} \quad (32)$$

$$= \exp \left(-\frac{\xi_i^2}{2\rho^2} \right),$$

283 and the supremum is reached at $\nu = -\exp \left(-\frac{\xi_i^2}{2\rho^2} \right)$.

284 From Eq. (26) and (32), we obtain:

$$\begin{aligned} \min J(\mathbf{p}_g, \xi_i, \nu_i) &= \frac{\lambda}{2} \mathbf{p}_g^T \mathbf{p}_g \\ &+ \sum_{i=1}^N \left(1 - \sup_{\nu_i} \left\{ \exp \left(-\frac{\xi_i^2}{2\rho^2} \right) \nu_i - g(\nu_i) \right\} \right), \quad (33) \\ \text{s.t. } y_i - \mathbf{p}_g^T \Phi_{gi} &= \xi_i, \quad i = 1, 2, \dots, N, \end{aligned}$$

285 where N samples for $\boldsymbol{\nu} = (\nu_1, \nu_2, \dots, \nu_N)^T \in \mathbf{R}^{N \times 1}$. Eq. (33)
286 can also be simplified as:

$$\begin{aligned} \min J(\mathbf{p}_g, \xi_i, \nu_i) &= \frac{\lambda}{2} \mathbf{p}_g^T \mathbf{p}_g \\ &+ \sup_{\nu} \left\{ \sum_{i=1}^N \left(-\frac{\xi_i^2}{2\rho^2} \nu_i + g(\nu_i) \right) \right\}, \quad (34) \\ \text{s.t. } y_i - \mathbf{p}_g^T \Phi_{gi} &= \xi_i, \quad i = 1, 2, \dots, N. \end{aligned}$$

287 We use an alternating algorithm to solve Eq. (34). Fixing
288 $\mathbf{p}_g^{(n)}$ and $\boldsymbol{\xi}^{(n)}$ to optimize $\boldsymbol{\nu}^{(n+1)}$, Eq. (34) becomes:

$$\min J(\boldsymbol{\nu}^{(n+1)}) = \sum_{i=1}^N \left(-\frac{(\xi_i^{(n)})^2}{2\rho^2} \nu_i^{(n+1)} + g(\nu_i^{(n+1)}) \right), \quad (35)$$

289 where n is the n -th iteration, and $\xi_i^{(n)} = y_i - (\mathbf{p}_g^{(n)})^T \Phi_{gi}$, $i =$
290 $1, 2, \dots, N$. According to Eq. (29), the closed-form solutions
291 of Eq. (35) are:

$$\nu_i^{(n+1)} = -\exp \left(-\frac{(\xi_i^{(n)})^2}{2\rho^2} \right) < 0, \quad i = 1, 2, \dots, N. \quad (36)$$

292 Fixing $\boldsymbol{\nu}^{(n+1)}$ optimizes $\mathbf{p}_g^{(n+1)}$ and $\boldsymbol{\xi}^{(n+1)}$ by solving the
293 following formula:

$$\begin{aligned} \min J(\mathbf{p}_g^{(n+1)}, \boldsymbol{\xi}^{(n+1)}) &= \frac{\lambda}{2} (\mathbf{p}_g^{(n+1)})^T \mathbf{p}_g^{(n+1)} \\ &+ \sum_{i=1}^N \left(-\frac{(\xi_i^{(n+1)})^2}{2\rho^2} \nu_i^{(n+1)} \right) \quad (37) \\ \text{s.t. } y_i - \mathbf{p}_g^T \Phi_{gi} &= \xi_i, \quad i = 1, 2, \dots, N. \end{aligned}$$

294 According to Eq. (37), the Lagrangian function is:

$$\begin{aligned} L(\mathbf{p}_g^{(n+1)}, \boldsymbol{\xi}^{(n+1)}, \boldsymbol{\alpha}^{(n+1)}) &= \frac{\lambda}{2} (\mathbf{p}_g^{(n+1)})^T \mathbf{p}_g^{(n+1)} \\ &+ \sum_{i=1}^N \left(-\frac{(\xi_i^{(n+1)})^2}{2\rho^2} \nu_i^{(n+1)} \right) \quad (38) \\ &- \sum_{i=1}^N \alpha_i^{(n+1)} \left(\xi_i^{(n+1)} - y_i + (\mathbf{p}_g^{(n+1)})^T \Phi_{gi} \right). \end{aligned}$$

We set the diagonal matrix $\mathbf{V}^{(n+1)} =$ 295
 $\text{diag}(-\nu_1^{(n+1)}, -\nu_2^{(n+1)}, \dots, -\nu_N^{(n+1)}) \in \mathbf{R}^{N \times N}$, and $\mathbf{y} =$ 296
 $(y_1, y_2, \dots, y_N)^T$, $\boldsymbol{\xi}^{(n+1)} = (\xi_1^{(n+1)}, \xi_2^{(n+1)}, \dots, \xi_N^{(n+1)})^T \in$ 297
 $\mathbf{R}^{N \times 1}$. Then, Eq. (38) can be simplified as: 298

$$\begin{aligned} L(\mathbf{p}_g^{(n+1)}, \boldsymbol{\xi}^{(n+1)}, \boldsymbol{\alpha}^{(n+1)}) &= \frac{\lambda}{2} (\mathbf{p}_g^{(n+1)})^T \mathbf{p}_g^{(n+1)} \\ &+ \frac{1}{2\rho^2} (\boldsymbol{\xi}^{(n+1)})^T \mathbf{V}^{(n+1)} \boldsymbol{\xi}^{(n+1)} \quad (39) \\ &+ (\boldsymbol{\alpha}^{(n+1)})^T \left(\mathbf{y} - ((\mathbf{p}_g^{(n+1)})^T \Phi_g)^T - \boldsymbol{\xi}^{(n+1)} \right). \end{aligned}$$

The partial derivatives of L is found by:: 299

$$\begin{cases} \frac{\partial L}{\partial \boldsymbol{\xi}^{(n+1)}} = 0 & \Rightarrow \boldsymbol{\xi}^{(n+1)} = \rho^2 (\mathbf{V}^{(n+1)})^{-1} \boldsymbol{\alpha}^{(n+1)}, \\ \frac{\partial L}{\partial \mathbf{p}_g^{(n+1)}} = 0 & \Rightarrow \mathbf{p}_g^{(n+1)} = \frac{1}{\lambda} \Phi_g \boldsymbol{\alpha}^{(n+1)}, \\ \frac{\partial L}{\partial \boldsymbol{\alpha}^{(n+1)}} = 0 & \Rightarrow \mathbf{y} - ((\mathbf{p}_g^{(n+1)})^T \Phi_g)^T = \boldsymbol{\xi}^{(n+1)}. \end{cases} \quad (40)$$

Similar to KHFIS, Eq. (40) is the solution of C-KHFIS 300
and belongs to the supervised learning stage of our algorithm,
which uses the error to learn parameters. We can obtain $\boldsymbol{\alpha}^{(n+1)}$ 301
and $\mathbf{p}_g^{(n+1)}$: 302
303

$$\begin{aligned} \boldsymbol{\alpha}^{(n+1)} &= \left(\frac{1}{\lambda} (\Phi_g)^T \Phi_g + \rho^2 (\mathbf{V}^{(n+1)})^{-1} \right)^{-1} \mathbf{y} \\ &= \left(\frac{1}{\lambda} \boldsymbol{\Omega} + \rho^2 (\mathbf{V}^{(n+1)})^{-1} \right)^{-1} \mathbf{y}. \end{aligned} \quad (41)$$

$$\mathbf{p}_g^{(n+1)} = \frac{1}{\lambda} \Phi_g \left(\frac{1}{\lambda} \boldsymbol{\Omega} + \rho^2 (\mathbf{V}^{(n+1)})^{-1} \right)^{-1} \mathbf{y}. \quad (42)$$

The process of C-KHFIS is listed in Algorithm 2. Theorem 304
1 indicates that Algorithm 2 converges. 305

Theorem 1: The values of Eq. (33) monotonically decrease 306
in each iteration until convergence. 307

Proof 1: Suppose $J(\mathbf{p}_g^{(n)}, \boldsymbol{\xi}^{(n)}, \boldsymbol{\nu}^{(n)})$ is the value of the 308
objective function Eq. (33) in the n -th iteration. In the $(n+1)$ -th 309
iteration, $\mathbf{p}_g^{(n)}$ is fixed, and the subproblem Eq. (35) is 310
solved to obtain the optimal $\boldsymbol{\nu}^{(n+1)}$. Since Eq. (35) is convex, 311
then 312

$$J(\mathbf{p}_g^{(n)}, \boldsymbol{\xi}^{(n)}, \boldsymbol{\nu}^{(n+1)}) \leq J(\mathbf{p}_g^{(n)}, \boldsymbol{\xi}^{(n)}, \boldsymbol{\nu}^{(n)}). \quad (43)$$

Fixing $\boldsymbol{\nu}^{(n+1)}$ and solving Eq. (37) via Eq. (42), we can achieve 313
the optimal $\mathbf{p}_g^{(n+1)}$ in the $(n+1)$ -th iteration. Eq. (37) is 314
convex problem, so we have 315

Algorithm 2 Algorithm of C-KHFIS

Require: The training labels $\mathbf{y} \in \mathbf{R}^{N \times 1}$, features $\mathbf{X} = [\mathbf{x}_1, \dots, \mathbf{x}_i, \dots, \mathbf{x}_N] \in \mathbf{R}^{d \times N}$ and testing sample $\mathbf{x}_t \in \mathbf{R}^{d \times 1}$; The parameters of regularization coefficient λ , number of fuzzy rules M and width ρ ;

Ensure: The prediction of $y(\mathbf{x}_t)$;

- 1: Using FCM to calculate the parameters of if-parts;
- 2: Estimating $\tilde{\mu}^k(\mathbf{x}_i), i = 1, 2, \dots, N, k = 1, 2, \dots, M$ by Eq. (3a) and (3b);
- 3: Computing Ω by Eq. (22) and (21);
- 4: Randomly initializing $\alpha^{(1)}$;
- 5: **for** $n = 1 \rightarrow n_{max}$ **do**
- 6: Calculating $\xi^{(n)}$ by $\xi^{(n)} = \Omega \alpha^{(n)} - \mathbf{y}$;
- 7: Estimating $\nu_i^{(n+1)}, i = 1, 2, \dots, N$ by Eq. (36);
- 8: Constructing $\mathbf{V}^{(n+1)} = \text{diag}(-\nu_1^{(n+1)}, -\nu_2^{(n+1)}, \dots, -\nu_N^{(n+1)})$;
- 9: Calculating $\alpha^{(n+1)} = \left(\frac{1}{\lambda} \Omega + \rho^2 (\mathbf{V}^{(n+1)})^{-1}\right)^{-1} \mathbf{y}$;
- 10: **end for**
- 11: Predicting $y(\mathbf{x}_t)$ by Eq. (23);

$$J(\mathbf{p}_g^{(n+1)}, \xi^{(n+1)}, \nu^{(n+1)}) \leq J(\mathbf{p}_g^{(n)}, \xi^{(n)}, \nu^{(n)}). \quad (44)$$

316 Finally, we combine the above results and obtain the
317 following:

$$J(\mathbf{p}_g^{(n+1)}, \xi^{(n+1)}, \nu^{(n+1)}) \leq J(\mathbf{p}_g^{(n)}, \xi^{(n)}, \nu^{(n)}). \quad (45)$$

318 *C. Robustness analysis*

319 To verify the robustness of C-KHFIS, we employ two
320 experiments, which include classification and regression. The
321 noise samples will affect the construction of the model and
322 lead to poor prediction performance. In Fig. 3(a), we randomly
323 generate two classes (blue and red points) of data under a
324 Gaussian distribution. Each class contains 300 samples. C-
325 KHFIS, KHFIS and 1-FIS have similar classification decision
326 boundaries and separate the two classes easily. In Fig. 3(b), 50
327 noise points are added to the data set. The 50 noise samples
328 original belong to class 2. However, these points are regarded as
329 class 1. With the addition of noise, the decision boundaries of
330 the three models all change. The changes in KHFIS and 1-FIS
331 are obvious. Due to the suppression of the robust loss function,
332 the decision boundary of C-KHFIS is almost unaffected. In
333 Fig. 4(a), there is no noise in the data set, which is generated
334 by the sinc function. Each model has a good fitting effect. In
335 Fig. 4(b), 30 random noise points are added to the original
336 data set. The performance of each method is affected. Due
337 to the kernel method (nonlinear), C-KHFIS and KHFIS are
338 less affected than the 1-FIS method. Compared with KHFIS,
339 C-KHFIS has a better fitting effect.

340 **IV. THE FEATURE EXTRACTION OF DNA SEQUENCES**

341 In this work, we utilize position-specific trinucleotide se-
342 quence propensity (PSTNP) [6] to represent the features of
343 DNA sequences. PSTNP is the extended version of pseudo
344 K-tuple nucleotide composition (PseKNC) [38], [39], [40]. The
345 DNA sequence generally includes four characters: 'A', 'C', 'G',

and 'T'. PSTNP generally uses trinucleotide (TriN) to locally
represent DNA sequences. The trinucleotide can be expressed
as:

$$\begin{cases} TriN_1 & = 'AAA'; \\ TriN_2 & = 'AAC'; \\ TriN_3 & = 'AAG'; \\ & \dots; \\ TriN_{64} & = 'TTT'; \end{cases} \quad (46)$$

To represent a DNA sequence containing 4mC sites, a
PSTNSP profile is defined as:

$$C_{i,j} = F^+(TriN_i|j) - F^-(TriN_i|j), \quad (47)$$

$$i = 1, 2, \dots, 64; j = 1, 2, \dots, 39,$$

where i is the type of trinucleotide and j denotes the position
on the 4mC fragment. $F^+(TriN_i|j)$ and $F^-(TriN_i|j)$ are
the frequencies of the i -th trinucleotide of the j -th position
for positive and negative samples, respectively. The length of
the 4mC fragment was 41 in He's study [6].

356 **V. EXPERIMENTS AND RESULTS**

357 *A. Data sets of 4mC*

358 In Chen's work [5], six types of data sets were collected.
359 There were Escherichia coli (E.coli), Caenorhabditis elegans
360 (C.elegans), Geobacter pickeringii (G.pickeringii), Arabidopsis thaliana
361 (A.thaliana) and Drosophila melanogaster (D.melanogaster).
362 The sizes of the six data sets are listed in Table I. Readers can
363 refer to Chen's work [5] for the construction process.
364

TABLE I: The size of the 4mC data sets .

Species	Negative	Positive
A.thaliana	1,978	1,978
C.elegans	1,554	1,554
D.melanogaster	1,769	1,769
E.coli	388	388
G.pickeringii	569	569
G.subterraneus	906	906

365 *B. Measurement of performance*

366 Matthew's correlation coefficient (MCC), sensitivity (SN),
367 specificity (SP) and accuracy (ACC) are employed to evaluate
368 the models. They are:

$$MCC = \frac{TP \times TN - FP \times FN}{\sqrt{(TP + FN) \times (TN + FP) \times (TP + FP) \times (TN + FN)}}, \quad (48a)$$

$$SN = \frac{TP}{FN + TP}, \quad (48b)$$

$$Spec = \frac{TN}{FP + TN}, \quad (48c)$$

$$ACC = \frac{TN + TP}{TN + FN + TP + FP}, \quad (48d)$$

$$(48e)$$

369 , where FP , FN , TN and TP are the numbers of false
370 positives, false negatives, true negatives and true positives,
371 respectively. Ten-fold cross-validation (10-CV) is utilized to
372 verify the performance of classifiers.

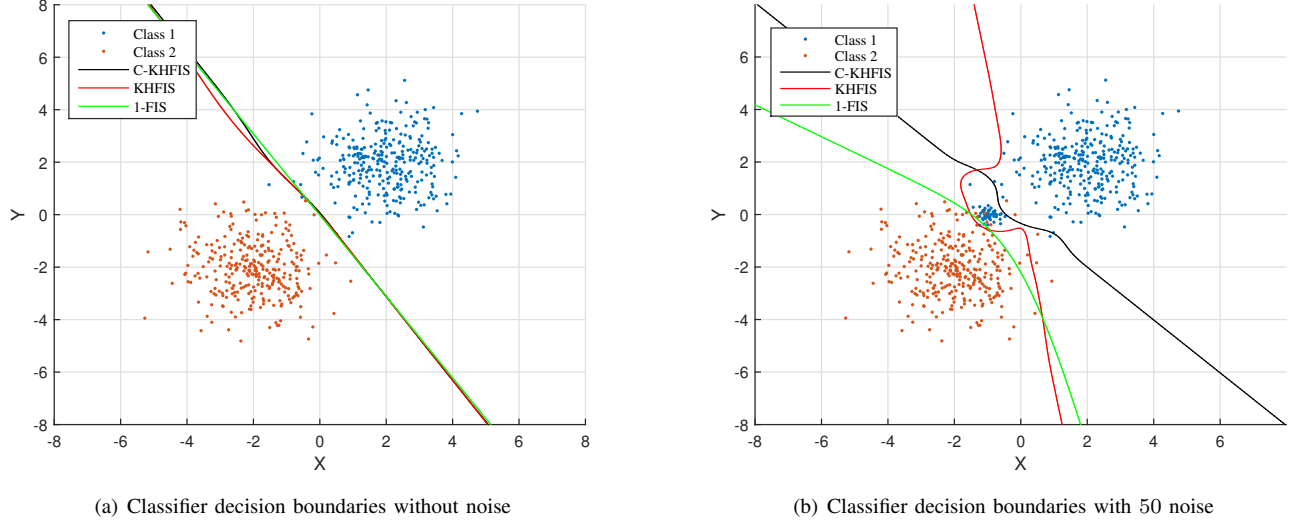


Fig. 3: The decision boundaries of different models.

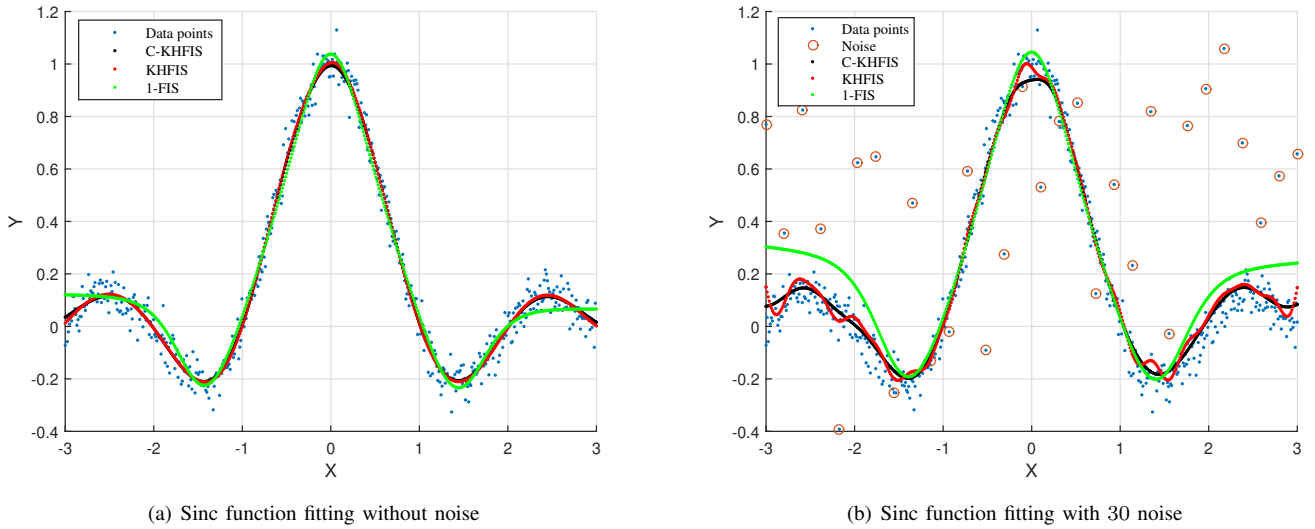


Fig. 4: The sinc function fitting curves of different models.

373 *C. Convergence on 4mC data sets*

374 The convergence of C-KHFIS is also verified by means of
 375 experimental simulation. In Fig. 5, we calculate the objective
 376 value of C-KHFIS in each iteration. On all data sets, the C-
 377 KHFIS model can converge after 4 iterations. Therefore, our
 378 optimization algorithm is effective and the convergence speed
 379 of the C-KHFIS is fast.

380 *D. Comparison of FIS methods*

381 To show the robustness of C-KHFIS, we evaluate the
 382 performance of 1-FIS, KHFIS and C-KHFIS. The results of
 383 the comparison are shown in Table II. In all data sets, the
 384 kernel-based models (with RBF kernel) have higher accuracy.
 385 Compared with 1-FIS, KHFIS has improved ACC by 0.75%,
 386 3.19%, 1.13%, 2.52%, 3.19% and 1.8% on the six data sets,

respectively. In Fig. 6, the area under the receiver operating
 characteristic (AUC) curves also show the classification per-
 formance of the models. On the six data sets, the C-KHFIS
 achieves the best AUCs of 0.8944, 0.9392, 0.9394, 0.9891,
 0.9621 and 0.9512, respectively.

392 *E. Comparison with existing predictors for 4mC*

393 Our method is compared with common 4mC predic-
 394 tion model. These methods include 4mCPred [6], Meta-
 395 4mCpred[11], iDNA4mC [5], 4mCpred-SVM [7], DeepTorrent
 396 [15] and 4mCNN [13]. The classifiers of the above methods
 397 mainly consist of SVM and convolutional neural network
 398 (CNN). It can be seen from Table III that our method obtains
 399 the best prediction accuracy on 6 data sets. Compared with
 400 the second-best method (DeepTorrent [15]), C-KHFIS improves

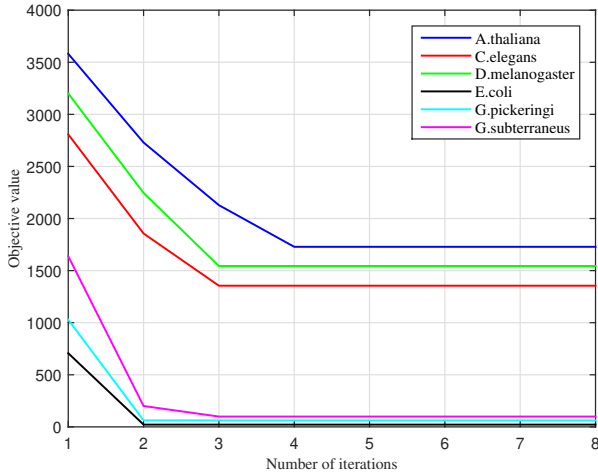


Fig. 5: The convergence curves of C-KHFIS on the 4mC data sets.

TABLE II: Comparison of the prediction performance between different FISs on six data sets (under 10-CV).

Species	Method	ACC	SN	SP	MCC
A.thaliana	1-FIS	0.7951	0.8270	0.7630	0.5909
	KHFIS	0.8026	0.7897	0.8155	0.6055
	C-KHFIS	0.8270	0.8181	0.8356	0.6537
C.elegans	1-FIS	0.8239	0.8283	0.8211	0.6493
	KHFIS	0.8558	0.8651	0.8517	0.7128
	C-KHFIS	0.8692	0.8632	0.8769	0.7398
D.melanogaster	1-FIS	0.8390	0.8585	0.8191	0.6784
	KHFIS	0.8503	0.8407	0.8593	0.7011
	C-KHFIS	0.8712	0.8726	0.8692	0.7421
E.coli	1-FIS	0.9218	0.9405	0.8991	0.8441
	KHFIS	0.9470	0.9510	0.9390	0.8941
	C-KHFIS	0.9529	0.9616	0.9410	0.9056
G.pickeringi	1-FIS	0.8545	0.8795	0.8308	0.7104
	KHFIS	0.8864	0.8818	0.8923	0.7732
	C-KHFIS	0.9039	0.9032	0.9053	0.8083
G.subterraneus	1-FIS	0.8438	0.8619	0.8261	0.6894
	KHFIS	0.8618	0.8608	0.8639	0.7238
	C-KHFIS	0.8903	0.8866	0.8944	0.7812

ACC by 2.4%, 1.1%, 1%, 8%, 1% and 1%, respectively, on six data sets. DeepTorrent [15] was built based on a deep learning model, which was good at feature representation learning. However, the recognition rate of positive samples is much lower than that of negative samples on multiple data sets. As a result, the value of SP is much higher than that of other machine learning methods. Deep learning requires more samples to train the parameters of the network. When the number of samples is small and the selection of initialization parameters is unreasonable, the prediction results will be biased. Moreover, the loss function of the model is important. The C loss function is a bounded, nonconvex, smooth loss function. C-KHFIS is a C loss-based neuro-fuzzy systems that can effectively reduce the impact of outliers on classification. The gap between SN and SP is not very large.

TABLE III: Comparison between different methods on six data sets (under 10-CV).

Species	Method	ACC	SN	SP	MCC
A.thaliana	Meta-4mCpred[11]	0.792	0.761	0.822	0.584
	4mCPred [6]	0.768	0.755	0.780	0.536
	iDNA4mC [5]	0.760	0.757	0.762	0.519
	4mCNN [13]	0.797	0.804	0.792	0.623
	4mCPred-SVM [7]	0.787	0.778	0.796	0.573
	DeepTorrent [15]	0.803	0.703	0.903	0.620
	C-KHFIS	0.827	0.818	0.836	0.654
C.elegans	Meta-4mCpred[11]	0.826	0.840	0.812	0.652
	4mCPred [6]	0.826	0.825	0.826	0.652
	iDNA4mC [5]	0.786	0.797	0.775	0.572
	4mCNN [13]	0.842	0.895	0.825	0.694
	4mCPred-SVM [7]	0.815	0.824	0.807	0.631
	DeepTorrent [15]	0.858	0.810	0.906	0.719
	C-KHFIS	0.869	0.863	0.877	0.740
D.melanogaster	Meta-4mCpred[11]	0.842	0.831	0.854	0.685
	4mCPred [6]	0.822	0.824	0.821	0.646
	iDNA4mC [5]	0.812	0.833	0.791	0.625
	4mCNN [13]	0.854	0.864	0.854	0.687
	4mCPred-SVM [7]	0.830	0.838	0.822	0.661
	DeepTorrent [15]	0.861	0.834	0.889	0.724
	C-KHFIS	0.871	0.873	0.869	0.742
E.coli	Meta-4mCpred[11]	0.848	0.869	0.827	0.697
	4mCPred [6]	0.826	0.819	0.832	0.655
	iDNA4mC [5]	0.799	0.820	0.778	0.598
	4mCNN [13]	0.859	0.881	0.789	0.688
	4mCPred-SVM [7]	0.833	0.858	0.807	0.666
	DeepTorrent [15]	0.873	0.891	0.855	0.747
	C-KHFIS	0.953	0.962	0.941	0.906
G.pickeringi	Meta-4mCpred[11]	0.891	0.884	0.898	0.782
	4mCPred [6]	0.830	0.850	0.810	0.668
	iDNA4mC [5]	0.831	0.824	0.838	0.663
	4mCNN [13]	0.872	0.858	0.893	0.750
	4mCPred-SVM [7]	0.860	0.863	0.858	0.721
	DeepTorrent [15]	0.894	0.831	0.957	0.795
	C-KHFIS	0.904	0.903	0.905	0.808
G.subterraneus	Meta-4mCpred[11]	0.855	0.856	0.854	0.711
	4mCPred [6]	0.828	0.818	0.837	0.662
	iDNA4mC [5]	0.815	0.822	0.808	0.630
	4mCNN [13]	0.860	0.852	0.843	0.704
	4mCPred-SVM [7]	0.837	0.840	0.837	0.674
	DeepTorrent [15]	0.880	0.813	0.948	0.768
	C-KHFIS	0.890	0.887	0.894	0.781

F. Comparison on UCI data sets

We further utilize eight data sets to evaluate KHFIS and C-KHFIS from the UCI Machine Learning Repository [41]. KNN, standard SVM [42], Kernel sparse representation-based classifier (Kernel SRC) [43] and 1-FIS are performed on these data via 5-CV. The results of the comparison are shown in Table IV. C-KHFIS achieves the highest values of accuracy on Australian (0.8757), ionosphere (0.9601), breast (0.9801), blood (0.8002), hearts (0.8519), diabetes (0.7834), and sonar (0.9150) data sets. In addition, Kernel SRC has the best accuracy (0.7740) on German Credit. C-KHFIS is also competent in other fields.

VI. CONCLUSION AND FUTURE WORK

In this study, we employ the position-specific trinucleotide sequence propensity method to extract key information from DNA sequences, propose the C-KHFIS model to construct a classifier, and achieve competitive results. PSTNP can estimate

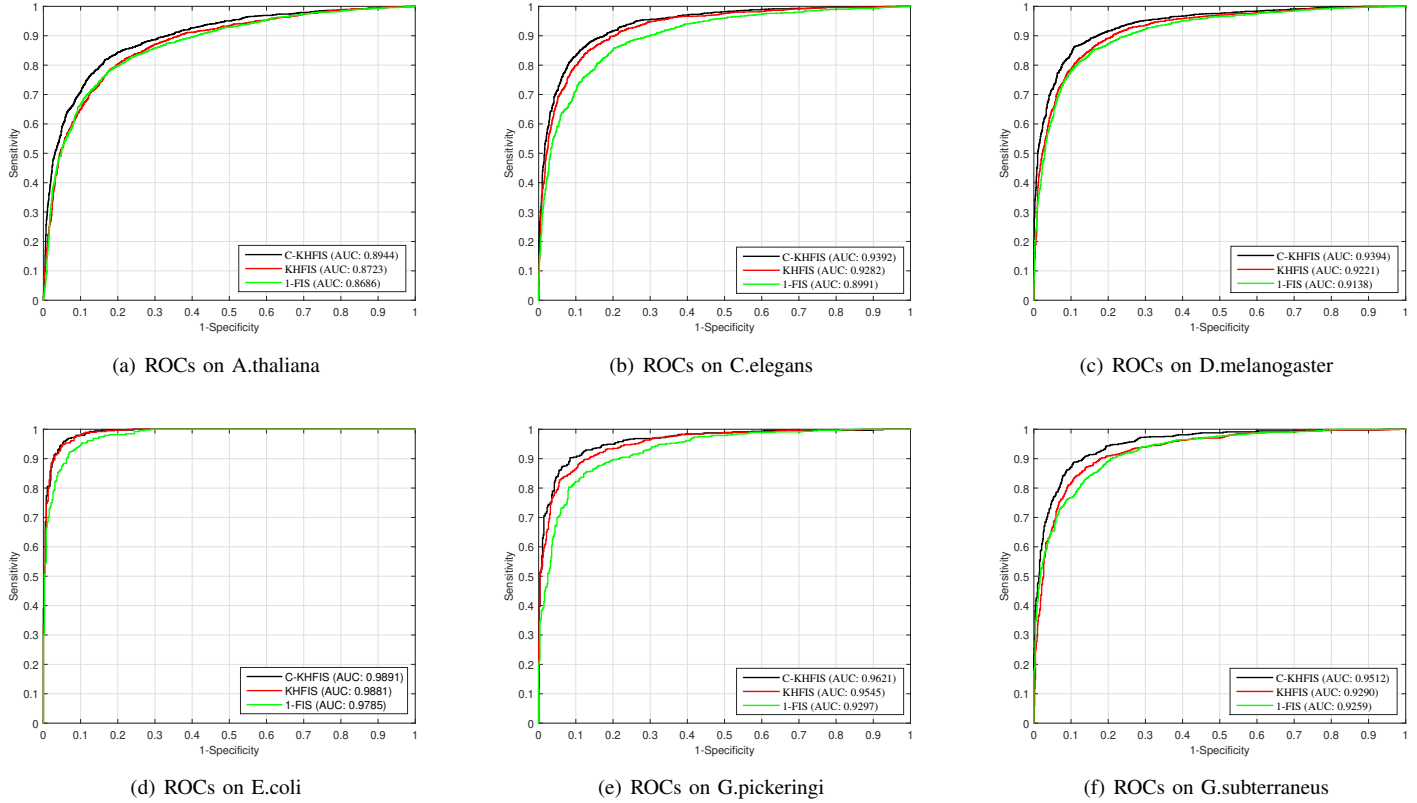


Fig. 6: The ROCs of different models.

TABLE IV: The accuracy of different classifiers on UCI data sets.

Data set	KNN	RF	SVM	Kernel SRC	1-FIS	KHFIS	C-KHFIS
Australian	0.8565	0.8638	0.8623	0.8304	0.8609	0.8638	0.8757
Blood	0.7888	0.7687	0.7861	0.7928	0.7686	0.7861	0.8002
Breast Cancer Wisconsin (Original)	0.9722	0.9751	0.9736	0.9634	0.9327	0.9678	0.9801
Diabetes	0.7552	0.7591	0.7773	0.7785	0.7760	0.7708	0.7834
German Credit	0.7330	0.7690	0.7630	0.7740	0.7650	0.7660	0.7730
Hearts	0.8222	0.8370	0.8370	0.8037	0.8370	0.8407	0.8519
Ionosphere	0.8547	0.9430	0.9544	0.8746	0.8832	0.9459	0.9601
Sonar	0.8510	0.9002	0.8702	0.8942	0.8221	0.9038	0.9150

433 the composition of each nucleotide at each position of DNA
 434 sequences. In the data sets of 4mC sites, there are always
 435 some noise samples (outliers) that will affect the hyperplane
 436 of classification. C-KHFIS is a C loss-based neuro-fuzzy
 437 systems that can effectively reduce the impact of outliers on
 438 classification. In Tables III and IV, it can be seen that the C
 439 loss function plays a good role in improving the performance of
 440 4mC prediction. We first employ a kernel trick to solve higher-
 441 order fuzzy inference systems and propose kernelized higher-
 442 order fuzzy inference systems (KHFIS), which have a good
 443 ability to solve nonlinear fitting. Then, the extended KHFIS,
 444 which is called the correntropy induced loss based KHFIS (C-
 445 KHFIS), is developed to reduce the influence of noise samples
 446 on the model. From the results in Fig. 3 and Fig. 4, it can be
 447 found that C-loss plays a good role in reducing the influence
 448 of noise. The experimental results of 4mC show that C-KHFIS
 449 achieves the best ACC on *A.thaliana* (0.827), *C.elegans* (0.869),
 450 *D.melanogaster* (0.871), *E.coli* (0.953), *G.pickeringi* (0.904),

and *G.subterraneus* (0.890). Moreover, C-KHFIS has good
 results on eight UCI data sets. The introduction of the kernel
 and C-loss method has greatly improved 1-FIS.

The 4mC site prediction is an important research direction
 in DNA sequence analysis. The accuracy of biological data
 affects the processing of the data. Therefore, high-quality
 4mC site samples are the key to building high-precision
 prediction models. The size of the training set is another factor
 in developing new predictors. Therefore, fuzzy systems (C-
 KHFIS) are very suitable for solving the problem of small
 samples and noisy samples. In addition, the introduction of
 multimodal DNA information is also a method to improve the
 prediction performance of 4mC sites.

In fact, a variety of information sources and features can be
 used to describe an object. To further improve the recognition
 accuracy of 4mC, more features and information can be
 introduced. Future work can consider multi-kernel learning
 [44], [45], [46] and multi-view learning [32], [47] to effectively

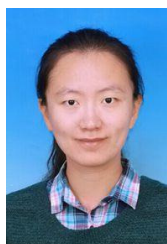
451
452
453
454
455
456
457
458
459
460
461
462
463
464
465
466
467
468

469 fuse features and further improve the prediction performance
470 of the FIS model.

REFERENCES

- 471
- 472 [1] B. Manavalan, M. Hasan, S. Basith, V. Gosu, T. Shin, and G. Lee,
473 “Empirical comparison and analysis of web-based dna n4-methylcytosine
474 site prediction tools,” *Mol Ther Nucleic Acids*, vol. 22, pp. 406–420,
475 2020.
- 476 [2] M. Hasan, W. Shoombuatong, H. Kurata, and B. Manavalan, “Critical
477 evaluation of web-based dna n6-methyladenine site prediction tools,”
478 *Briefings in Functional Genomics*, vol. 20, no. 4, pp. 258–272, 2021.
- 479 [3] M. Hasan, S. Basith, M. Khatun, G. Lee, B. Manavalan, and H. Ku-
480 rata, “Meta-i6ma: an interspecies predictor for identifying dna n6-
481 methyladenine sites of plant genomes by exploiting informative features in
482 an integrative machine-learning framework,” *Briefings in Bioinformatics*,
483 vol. 22, no. 3, p. bbaa202, 2021.
- 484 [4] C. Cortes and V. Vapnik, “Support-vector networks,” *Machine Learning*,
485 vol. 20, no. 3, pp. 273–297, 1995.
- 486 [5] W. Chen, H. Yang, P. Feng, H. Ding, and H. Lin, “iDNA4mC:
487 identifying DNA N4-methylcytosine sites based on nucleotide chemical
488 properties,” *Bioinformatics*, vol. 33, no. 22, pp. 3518–3523, 07 2017.
489 [Online]. Available: <https://doi.org/10.1093/bioinformatics/btx479>
- 490 [6] W. He, C. Jia, and Q. Zou, “4mcpred: machine learning methods for
491 dna n4-methylcytosine sites prediction.” *Bioinformatics*, vol. 35, no. 4,
492 pp. 593–601, 2019.
- 493 [7] L. Wei, S. Luan, L. A. E. Nagai, R. Su, and Q. Zou,
494 “Exploring sequence-based features for the improved prediction of
495 DNA N4-methylcytosine sites in multiple species,” *Bioinformatics*,
496 vol. 35, no. 8, pp. 1326–1333, 09 2018. [Online]. Available:
497 <https://doi.org/10.1093/bioinformatics/bty824>
- 498 [8] M. M. Hasan, B. Manavalan, M. S. Khatun, and H. Kurata, “i4mc-rose,
499 a bioinformatics tool for the identification of dna n4-methylcytosine
500 sites in the rosaceae genome,” *International Journal of Biological*
501 *Macromolecules*, vol. 157, pp. 752–758, 2020.
- 502 [9] M. Hasan, B. Manavalan, W. Shoombuatong, M. Khatun, and H. Kurata,
503 “i4mc-mouse: Improved identification of dna n4-methylcytosine sites in
504 the mouse genome using multiple encoding schemes,” *Computational*
505 *and Structural Biotechnology Journal*, vol. 18, pp. 906–912, 2020.
- 506 [10] H. Lv, F.-Y. Dao, D. Zhang, Z.-X. Guan, H. Yang, W. Su, M.-L. Liu,
507 H. Ding, W. Chen, and H. Lin, “idna-ms: an integrated computational
508 tool for detecting dna modification sites in multiple genomes,” *iScience*,
509 vol. 23, p. 100991, 2020.
- 510 [11] B. Manavalan, S. Basith, T. H. Shin, L. Wei, and G. Lee, “Meta-4mcpred:
511 A sequence-based meta-predictor for accurate dna 4mc site prediction
512 using effective feature representation,” *Mol Ther Nucleic Acids*, vol. 16,
513 pp. 733–744, 2019.
- 514 [12] Q. Tang, J. Kang, J. Yuan, H. Tang, X. Li, H. Lin, J. Huang, and W. Chen,
515 “Dna4mc-lip: a linear integration method to identify n4-methylcytosine
516 site in multiple species,” *Bioinformatics*, vol. 36, pp. 733–744, 2020.
- 517 [13] J. Khanal, I. Nazari, H. Tayara, and K. T. Chong, “4mccn: Identification
518 of n4-methylcytosine sites in prokaryotes using convolutional neural
519 network,” *IEEE Access*, vol. 7, pp. 145 455–145 461, 2019.
- 520 [14] A. Wahab, O. Mahmoudi, J. Kim, and K. T. Chong, “Dnc4mc-deep:
521 Identification and analysis of dna n4-methylcytosine sites based on
522 different encoding schemes by using deep learning,” *Cells*, vol. 9, no. 8,
523 p. 1756, 2020.
- 524 [15] Q. Liu, J. Chen, Y. Wang, S. Li, C. Jia, J. Song, and F. Li, “DeepTorrent:
525 a deep learning-based approach for predicting DNA N4-methylcytosine
526 sites,” *Briefings in Bioinformatics*, 07 2020, bbaa124. [Online]. Available:
527 <https://doi.org/10.1093/bib/bbaa124>
- 528 [16] Mamdani, “Application of fuzzy logic to approximate reasoning using
529 linguistic synthesis,” *IEEE Transactions on Computers*, vol. C-26, no. 12,
530 pp. 1182–1191, 1977.
- 531 [17] T. Takagi and M. Sugeno, “Fuzzy identification of systems and its
532 applications to modeling and control,” *IEEE Trans. Syst. Man Cybern.*,
533 vol. SMC-15, no. 1, p. 116–132, 1985.
- 534 [18] C.-J. Lin, “An efficient immune-based symbiotic particle swarm opti-
535 mization learning algorithm for tsk-type neuro-fuzzy networks design,”
536 *Fuzzy Sets and Systems*, vol. 159, no. 21, pp. 2890–2909, 2008.
- 537 [19] M. Azeem, M. Hanmandlu, and N. Ahmad, “Generalization of adaptive
538 neuro-fuzzy inference systems,” *IEEE Transactions on Neural Networks*,
539 vol. 11, no. 6, pp. 1332–1346, 2000.
- 540 [20] Y. Chen and J. Wang, “Support vector learning for fuzzy rule-based
541 classification systems,” *IEEE Transactions on Fuzzy Systems*, vol. 11,
542 no. 6, pp. 716–728, 2003.
- [21] J.-H. Chiang and P.-Y. Hao, “Support vector learning mechanism for
543 fuzzy rule-based modeling: a new approach,” *IEEE Transactions on*
544 *Fuzzy Systems*, vol. 12, no. 1, pp. 1–12, 2004.
- [22] P. Xu, Z. Deng, C. Cui, T. Zhang, K.-S. Choi, S. Gu, J. Wang, and
545 S. Wang, “Concise fuzzy system modeling integrating soft subspace
546 clustering and sparse learning,” *IEEE Transactions on Fuzzy Systems*,
547 vol. 27, no. 11, pp. 2176–2189, 2019.
- [23] Y. W. Kerk, K. M. Tay, and C. P. Lim, “Monotone fuzzy rule interpolation
548 for practical modelling of the zero-order tsf fuzzy inference system,”
549 *IEEE Transactions on Fuzzy Systems*, pp. 1–1, 2021.
- [24] Z. Deng, Y. Jiang, K.-S. Choi, F.-L. Chung, and S. Wang, “Knowledge-
550 leverage-based tsf fuzzy system modeling,” *IEEE Transactions on Neural*
551 *Networks and Learning Systems*, vol. 24, no. 8, pp. 1200–1212, 2013.
- [25] X. Gu, F.-L. Chung, and S. Wang, “Bayesian takagi-sugeno-kang fuzzy
552 classifier,” *IEEE Transactions on Fuzzy Systems*, vol. 25, no. 6, pp.
553 1655–1671, 2017.
- [26] B. Rezaee and M. F. Zarandi, “Data-driven fuzzy modeling for takagi-
554 sugeno-kang fuzzy system,” *Information Sciences*, vol. 180, no. 2, pp.
555 241–255, 2010.
- [27] H. Zuo, G. Zhang, W. Pedrycz, V. Behbood, and J. Lu, “Fuzzy regression
556 transfer learning in takagi-sugeno fuzzy models,” *IEEE Transactions on*
557 *Fuzzy Systems*, vol. 25, no. 6, pp. 1795–1807, 2017.
- [28] Z. Deng, Y. Cao, Q. Lou, K.-S. Choi, and S. Wang, “Monotonic relation-
558 constrained takagi-sugeno-kang fuzzy system,” *Information Sciences*, vol.
559 582, pp. 243–257, 2022.
- [29] H. Yu, J. Lu, and G. Zhang, “Topology learning-based fuzzy random
560 neural network for streaming data regression,” *IEEE Transactions on*
561 *Fuzzy Systems*, pp. 1–1, 2020.
- [30] D. Wu and J. M. Mendel, “Patch learning,” *IEEE Transactions on Fuzzy*
562 *Systems*, vol. 28, no. 9, pp. 1996–2008, 2020.
- [31] D. Wu, Y. Yuan, J. Huang, and Y. Tan, “Optimize tsf fuzzy systems for
563 regression problems: Minibatch gradient descent with regularization,
564 droprule, and adabound (mbgd-rda),” *IEEE Transactions on Fuzzy*
565 *Systems*, vol. 28, no. 5, pp. 1003–1015, 2020.
- [32] Y. Jiang, Z. Deng, F.-L. Chung, G. Wang, P. Qian, K.-S. Choi, and
566 S. Wang, “Recognition of epileptic eeg signals using a novel multiview
567 tsf fuzzy system,” *IEEE Transactions on Fuzzy Systems*, vol. 25, no. 1,
568 pp. 3–20, 2017.
- [33] Y. Jiang, D. Wu, Z. Deng, P. Qian, J. Wang, G. Wang, F.-L. Chung,
569 K.-S. Choi, and S. Wang, “Seizure classification from eeg signals using
570 transfer learning, semi-supervised learning and tsf fuzzy system,” *IEEE*
571 *Transactions on Neural Systems and Rehabilitation Engineering*, vol. 25,
572 no. 12, pp. 2270–2284, 2017.
- [34] K. Wiktorowicz and T. Krzeszowski, “Training high-order takagi-sugeno
573 fuzzy systems using batch least squares and particle swarm optimization,”
574 *International Journal of Fuzzy Systems*, vol. 22, p. 22–34, 2020.
- [35] A. Singh, R. Pokharel, and J. Principe, “The c-loss function for pattern
575 classification,” *Pattern Recognition*, vol. 47, no. 1, pp. 441–453, 2014.
- [36] J. C. Bezdek, R. Ehrlich, and W. Full, “Fcm: The fuzzy c-means clustering
576 algorithm,” *Computers and Geosciences*, vol. 10, no. 2, pp. 191–203,
577 1984.
- [37] Y. He, F. Wang, Y. Li, J. Qin, and B. Chen, “Robust matrix completion via
578 maximum coreentropy criterion and half-quadratic optimization,” *IEEE*
579 *Transactions on Signal Processing*, vol. 68, pp. 181–195, 2020.
- [38] W. Chen, H. Lin, and K.-C. Chou, “Pseudo nucleotide composition
580 or psekcnc: an effective formulation for analyzing genomic sequences,”
581 *Molecular BioSystems*, vol. 11, no. 10, pp. 2620–2634, 2015.
- [39] H. Lin, E.-Z. Deng, H. Ding, W. Chen, and K.-C. Chou, “ipro54-
582 psekcnc: a sequence-based predictor for identifying sigma-54 promoters
583 in prokaryote with pseudo k-tuple nucleotide composition,” *Molecular*
584 *BioSystems*, vol. 42, no. 21, pp. 12 961–12 972, 2014.
- [40] H. Lin, Z.-Y. Liang, H. Tang, and W. Chen, “Identifying sigma70
585 promoters with novel pseudo nucleotide composition,” *IEEE/ACM*
586 *Transactions on Computational Biology and Bioinformatics*, vol. 16,
587 no. 4, pp. 1316–1321, 2019.
- [41] D. Dua and C. Graff, “Uci machine learning repository,” 2017. [Online].
588 Available: <http://archive.ics.uci.edu/ml>
- [42] C.-C. Chang and C.-J. Lin, “LIBSVM: A library for support vector
589 machines,” *ACM Transactions on Intelligent Systems and Technology*,
590 vol. 2, pp. 27:1–27:27, 2011, software available at <http://www.csie.ntu.edu.tw/~cjlin/libsvm>.
- [43] L. Zhang, W. Zhou, P. Chang, J. Liu, Z. Yan, T. Wang, and F. Li,
591 “Kernel sparse representation-based classifier,” *IEEE Transactions on*
592 *Signal Processing*, vol. 60, no. 4, pp. 1684–1695, 2012.
- [44] Y. Ding, J. Tang, and G. Fei, “Identification of drug-side effect association
593 via multiple information integration with centered kernel alignment,”
594 *Neurocomputing*, vol. 325, pp. 211–224, 2019.

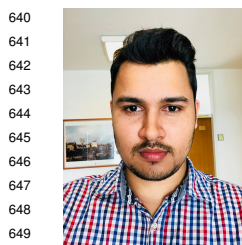
- 620 [45] Y. Ding, J. Tang, and F. Guo, "Human protein subcellular localization
 621 identification via fuzzy model on kernelized neighborhood representation,"
 622 *Applied Soft Computing*, vol. 96, p. 106596, 2020.
- 623 [46] H. Yang, Y. Ding, J. Tang, and F. Guo, "Drug-disease associations
 624 prediction via multiple kernel-based dual graph regularized least squares,"
 625 *Applied Soft Computing*, vol. 112, p. 107811, 2021.
- 626 [47] Y. Ding, J. Tang, and F. Guo, "Identification of drug-target interactions via
 627 multi-view graph regularized link propagation model," *Neurocomputing*,
 628 vol. 461, pp. 618–631, 2021.



671 **Fei Guo** received the bachelor degree and the PhD
 672 degree from Shandong University, in 2007 and 2012.
 673 She was a postdoctoral fellow at City University of
 674 Hong Kong between 2012 and 2013. She is currently
 675 a professor in the School of Computer Science and
 676 Engineering, Central South University. Her research
 677 interests include bioinformatics and computational
 678 biology.



629 **Yijie Ding** received his Ph.D. degree from the
 630 School of Computer Science and Technology at
 631 Tianjin University in 2018. Currently, he is an
 632 associate professor in the Yangtze Delta Region
 633 Institute (Quzhou), University of Electronic Science
 634 and Technology of China. His research interests
 635 include bioinformatics and machine learning. Several
 636 related works have been published by Briefings
 637 in Bioinformatics, IEEE/ACM TCBB, IEEE JBHI,
 638 Information Sciences, Knowledge-Based Systems,
 639 Applied Soft Computing and Neurocomputing.



640 **Prayag Tiwari** (Member, IEEE) received his Ph.D
 641 degree from the University of Padova, Italy. He is
 642 currently working as a Postdoctoral Researcher at the
 643 Aalto University, Finland. Previously, he was working
 644 as a Marie Curie Researcher at the University of
 645 Padova, Italy. He also worked as a research assistant
 646 at the NUST "MISiS", Moscow, Russia. He has
 647 several publications in top journals and conferences
 648 including, Neural Networks, Information Fusion,
 649 IPM, IJCV, IEEE TNNLS, IEEE TFS, IEEE TII,
 650 IEEE JBHI, IEEE IOTJ, IEEE BIBM, ACM TOIT,
 651 CIKM, SIGIR, AAAI, etc. His research interests include Machine Learning,
 652 Deep Learning, Quantum Machine Learning, Information Retrieval, Healthcare,
 653 and IoT.



680 **Prof. Hari Mohan Pandey** (Senior Member, IEEE)
 681 received the B.Tech. degree from Uttar Pradesh
 682 Technical University, India, the M.Tech. degree from
 683 the Narsee Monjee Institute of Management Studies,
 684 India, and the Ph.D. degree computer science and
 685 engineering from the Amity University, India. He
 686 worked as a Postdoctoral Research Fellow with the
 687 Middlesex University, London, U.K. He also worked
 688 on a European Commission project – Dream4car
 689 under H2020. He is a Senior Lecturer with the De-
 690 partment of Computer Science, Edge Hill University,
 691 Lancashire, U.K. He is 966 specialized in computer science and engineering
 692 and his research area includes, artificial intelligence, soft computing, natural
 693 language processing, language acquisition, machine learning, and deep learning.



654 **Quan Zou** is a professor of Institute of Fundamental
 655 and Frontier Sciences, University of Electronic Sci-
 656 ence and Technology of China. He received his PH.D.
 657 from Harbin Institute of Technology, P.R.China in
 658 2009, and worked at Xiamen University and Tianjin
 659 University from 2009 to 2018. His research is in
 660 the areas of bioinformatics, machine learning and
 661 parallel computing. Now he is putting the focus on
 662 protein classification, genome assembly, annotation
 663 and functional analysis from the next generation
 664 sequencing data with parallel computing methods.

665 Several related works have been published by Briefings in Bioinformatics,
 666 Bioinformatics, PLOS Computational Biology and IEEE/ACM Transactions
 667 on Computational Biology and Bioinformatics. Google scholar showed that
 668 his more than 100 papers have been cited more than 4000 times. He is the
 669 Editor-in-Chief of Current Bioinformatics. He is also a reviewer for many
 670 impacted journals and NSFC(National Natural Science Foundation of China).